An Optimal Steering Law for Sailing with Solar and Planetary Radiation Pressure

Anaïs Barles[a], Matteo Ceriotti[b], Francesco Ciampa[c], Leonard Felicetti[a*]

[a] *Cranfield University, Cranfield, Bedfordshire, MK43 0AL, United Kingdom*
[b] *University of Glasgow, Glasgow, G12 8QQ, United Kingdom*
[c] *University of Surrey, Guildford, GU2 7XH, United Kingdom*

Abstract

An optimal steering law for sails that exploit both solar and infrared planetary radiation pressure is presented in this paper. The optimal steering law maximises the orbit raise over one revolution of the sail around the planet. An indirect analytical approach, that uses Pontryagin Minimum Principle, is used to develop specialised steering laws for the sunlit and eclipse cases in a planar motion scenario. The law for the sunlit case uses both the solar and infrared radiation emitted from the planet, while the law for the eclipse case finds the optimal sail attitude that maximises the raise of the orbit using only the planetary radiation. Numerical results show that these laws lead to better performance in terms of orbit raising against other sub-optimal and optimal strategies exploiting the solar radiation pressure only. A numerical study is also carried out to show the effects of the reflectivity coefficient in the infrared band on the orbital motion of the sail.

Keywords: Solar Sail; Optimal Control; Pontryagin Minimum Principle; Solar Radiation; Planetary Infrared Radiation; Orbital Dynamics

1. Introduction

Most of the spacecraft propulsion systems are based on Newton's law of action-reaction: a reaction mass is accelerated in a high-velocity jet and produces thrust. However, since the beginning of space propulsion during the

* Corresponding author.
E-mail addresses: barles.anais13@gmail.com (A. Barles), Matteo.Ceriotti@glasgow.ac.uk (M. Ceriotti), f.ciampa@surrey.ac.uk (F. Ciampa), Leonard.Felicetti@cranfield.ac.uk (L. Felicetti)

1920s, the father of astronautics Konstantin Tsiolkovsky and his co-worker Fridrickh Tsander wrote about the idea that the pressure of sunlight could be used to attain high velocities thanks to ‘tremendous mirrors of very thin sheets’ [1]. It was not until the 1950s that this concept was reinvented by Carl Wiley: he highlighted the benefits of using solar sails, especially for interplanetary travels [1]. Indeed, space exploration has been highly limited by the reaction mass that has to be carried on board.

Solar sailing is a form of propulsion which is not subject to propellant mass limitations. Thus, the acceleration provided by solar sails is only limited by the lifetime of the sail film in the space environment. Indeed, sunlight is composed of photons that carry momentum, which can be transferred to the spacecraft through the use of solar sails to generate thrust.

However, due to the small amount of momentum carried by an individual photon, solar sails must have a large surface to maximise the number of photons that are reflected [1].

For a long time, solar sailing has remained theoretical and lots of different missions have been studied. Indeed, the acceleration of the sailcraft can be both reduced and increased by changing the orientation of the solar sail. Moreover, because of the unlimited and continuous acceleration provided, it enables a vast range of missions, as presented by Gong and Macdonald [2], both planetocentric and interplanetary. Focusing on the former, Macdonald and McInnes [3] highlighted that solar sailing could enable, or significantly improve, typical missions such as in non-inertially-fixed orbits: in the GeoSail mission concept [4], a near-continuous observation of the magnetosphere is made possible by a continuous drift of the orbit which maintains the payload alignment within the Earth’s geomagnetic tail.

Nevertheless, most studies only consider the force due to SRP. However, planets emit radiation and partially reflect the one that is coming from the Sun. Indeed, due to the thermodynamic equilibrium with its environment, the planet emits black-body radiation [5]. Moreover, the reflection of the radiation coming from the Sun is known as the albedo. This radiation varies both with the geological composition of the soil and seasons. Photons both emitted and reflected by planets hit the solar sail and can contribute to its acceleration, when the sail is in a planetary orbit.

A recent study by De Iuliis et al. [6] considered the contribution of both SRP and Planetary Radiation Pressure (PRP) to increase the semi-major axis. The work showed that the effect of the PRP on the acceleration of a planetary sail can be significant when performing an increase of the semi-major axis with a suboptimal control law. The aim of this paper is to extend previous work by searching for optimal laws that maximise the exploitation of both SRP and PRP for performing orbit-raising manoeuvres.

The PRP can be considered to be composed of two parts, the Albedo Radiation Pressure (ARP) and the Black-Body Radiation Pressure (BBRP). The main difference between these terms is that BBRP is the infrared radiation isotropically emitted by the planet, while the ARP is the sun-radiation reflected by the planet and, for this reason it depends on the relative geometry between the Sun, the planet and the sail. The aim of this work is to derive an optimal steering law to increase the semi-major axis of a solar sail exploiting both SRP and BBRP.. This work shows that the inclusion of the BBRP within the sail control law increases the performance of the sail especially when it is close to the planet.

The optimisation of planet-centered solar sails has been addressed in several works. Fieseler [7] proposed a sail configuration that allows operation in high-inclination Earth orbits from low inclination, despite the atmospheric drag. Macdonald and McInnes [8,9] blended locally-optimal control laws to perform planet-centred transfers and stationkeeping. Mengali and Quarta developed optimal laws to use a solar sail to raise low Earth orbit [10] and escape [11]. Stolbunov et al. [12] combined the effects of solar radiation pressure and atmospheric drag to determine an optimal control law for inclination change. Felicetti et al. [13] proposed raising an Earth orbit using a variable-geometry pyramid sail.

In this study, an indirect approach is adopted by using Pontryagin's Minimum Principle [14, 15], as it provides a semi-analytical control law by determining sufficient conditions for optimality. This method has been previously used, for example, by Mengali and Quarta [10] to determine an optimal control law for orbit raising from low Earth orbit. The same approach is applied in this study but with also the inclusion of the radial force due to the BBRP. This will result in a significant change in the optimal steering law of the sail, with an increase of the orbit raise performance.

This article is organised as follows: Section 2 presents the dynamical model of the sail in a planar case as well as the expressions of the acceleration due to both SRP and BBRP. In Section 3, optimal steering laws are derived to maximise the semi-major axis of the sail. Two different optimisation regimes are considered, related to different regions on the orbit: the sunlit region, where both SRP and BBRP are acting on the sail and the eclipse region, where only the BBRP is present. The numerical results in Section IV assess the performance of the optimal steering laws by comparison against other classical sub-optimal laws during one revolution, starting from a circular orbit, at different altitudes, and for two planets: Earth and Venus. The choice of Venus is due to its intense BBRP, as shown in Ref. [6]. Further, parametric studies quantify the sail's performance against its characteristic acceleration and optical properties

of the sail, showing that the reflectivity coefficient of both the sunlight and infrared radiation affects the performance of the sail. Final considerations and remarks are discussed in the Conclusion.

2. Solar and Planetary Sail Modelling

This section aims to describe the dynamics of the sail as well as define the forces exerted by the solar radiation pressure and the black-body radiation pressure.

2.1. Dynamical model

A flat solar sail orbiting in a circular orbit around a planet in a two-dimensional case is shown in Fig. 1. The x-axis of the planet-centred reference frame points towards the Sun and the y-axis is normal to x in the ecliptic plane. The motion of the sail is subject to three different forcing terms: gravity, SRP and BBRP. The position of the sail is determined by the state vector $\boldsymbol{x} = [r \quad u \quad v \quad \theta]^T$; the equations of motion are written in a polar form as:

$$\dot{r} = u \tag{1}$$

$$\dot{u} = \frac{v^2}{r} - \frac{\mu_p}{r^2} + a_{u,SRP} + a_{u,BBRP} \tag{2}$$

$$\dot{v} = -\frac{uv}{r} + a_{v,SRP} + a_{v,BBRP} \tag{3}$$

$$\dot{\theta} = \frac{v}{r} \tag{4}$$

where r is the distance between the centre of the planet and the sail, u and v are the radial and transversal velocities and θ is the angular coordinate of the sail along the orbit, measured from a reference direction. $a_{u,SRP}$ and $a_{v,SRP}$ are the components of the acceleration due to SRP along the radial and the transversal directions and $a_{u,BBRP}$ and $a_{v,BBRP}$ are those due to BBRP.

Fig. 1 also shows a sail-centred reference frame, where $\hat{\boldsymbol{u}}_{\boldsymbol{p}}$ is the unit vector representing the direction of the photons coming from the planet and $\hat{\boldsymbol{u}}_{\boldsymbol{t}}$ is the in-plane direction perpendicular to $\hat{\boldsymbol{u}}_{\boldsymbol{p}}$. The unit vector $\hat{\boldsymbol{n}}$ defines the normal of the sail. The unit vector $\hat{\boldsymbol{u}}_{\boldsymbol{s}}$ corresponds to the direction of the incident photons from the Sun. It is assumed that the solar rays are parallel due to the large distance from the Sun. The attitude of the sail is determined by the angle α which is the angle between the direction of the incident photons from the Sun $\hat{\boldsymbol{u}}_{\boldsymbol{s}}$ and the normal of the sail $\hat{\boldsymbol{n}}$. It is measured clockwise and $\alpha \in \left[-\frac{\pi}{2}, \frac{\pi}{2}\right]$. Attitude changes of the sail are considered to be instantaneous.

Two other angles are defined: α_{sun} which is the angle between $\hat{\boldsymbol{u}}_{\boldsymbol{p}}$ and $\hat{\boldsymbol{u}}_{\boldsymbol{s}}$ while α_N is the angle between $\hat{\boldsymbol{u}}_{\boldsymbol{p}}$ and the normal of the sail $\hat{\boldsymbol{n}}$. Therefore, the vector components of $\hat{\boldsymbol{n}}$ and $\hat{\boldsymbol{u}}_{\boldsymbol{s}}$ are defined in the $(\hat{\boldsymbol{u}}_{\boldsymbol{p}}, \hat{\boldsymbol{u}}_{\boldsymbol{t}})$ reference frame as follows:

$$\hat{\boldsymbol{n}} = \begin{bmatrix} \cos \alpha_N \\ \sin \alpha_N \end{bmatrix} \qquad \hat{\boldsymbol{u}}_{\boldsymbol{s}} = \begin{bmatrix} \cos \alpha_{sun} \\ \sin \alpha_{sun} \end{bmatrix} \tag{5}$$

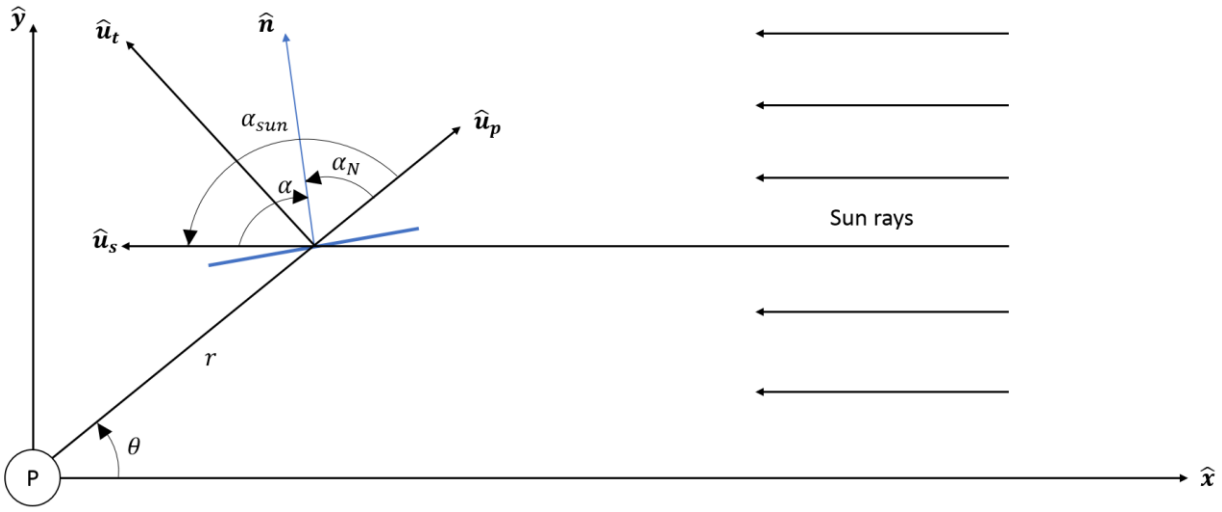

Fig. 1 Sail geometry and reference frames

2.2. Solar Radiation Pressure

The photon radiation pressure exerts a force on the sail which depends on three main parameters: the solar sail performance and both the direction and intensity of the incident photons. Indeed, as defined by McInnes [1], the acceleration on an ideal sail exerted along the normal $\hat{\boldsymbol{n}}$ by the incident and reflected photons is written as:

$$\boldsymbol{a_{SRP}} = \frac{2P_{sun}\eta_{SRP}}{\sigma}(\hat{\boldsymbol{u}}_{\boldsymbol{s}}.\hat{\boldsymbol{n}})^2\hat{\boldsymbol{n}} = a_0(\hat{\boldsymbol{u}}_{\boldsymbol{s}}.\hat{\boldsymbol{n}})^2\hat{\boldsymbol{n}} \tag{6}$$

where P_{sun} is the pressure locally exerted by the photons on the surface of the sail, η_{SRP} is the efficiency of the sail with respect to solar radiation pressure, $\sigma = m/A$ is the solar sail loading which represents the sail mass m per unit area A and $a_0 = \frac{2P_{sun}\eta_{SRP}}{\sigma}$ is the characteristic acceleration.

Eclipses are modelled considering a cylindrical shadow model (no penumbra). Therefore, the eclipse volume is represented as a cylinder with a radius equal to the planet and an axis opposite to the sun direction. In this volume, the SRP is not acting on the sail.

Finally, by substituting the expressions of $\hat{\boldsymbol{u}}_{\boldsymbol{s}}$ and $\hat{\boldsymbol{n}}$ in Eq. (5) into Eq. (6) and by considering that $\alpha_N = \alpha_{sun} - \alpha$, the expression of the acceleration due to the solar radiation pressure in the ($\hat{\boldsymbol{u}}_{\boldsymbol{p}}$, $\hat{\boldsymbol{u}}_{\boldsymbol{t}}$) reference frame is:

$$\boldsymbol{a}_{\boldsymbol{SRP}} = a_0 \cos^2\alpha \begin{bmatrix}\cos\alpha_N \\ \sin\alpha_N\end{bmatrix} = a_0 \cos^2\alpha \begin{bmatrix}\cos\alpha_{sun}\cos\alpha + \sin\alpha_{sun}\sin\alpha \\ \sin\alpha_{sun}\cos\alpha - \cos\alpha_{sun}\sin\alpha\end{bmatrix} \tag{7}$$

2.3. Black-Body Radiation Pressure

Planets can be considered as black bodies in equilibrium with their environment. Therefore, they are emitting the so-called black body radiation according to the Stefan-Boltzmann law [6]:

$$L_{P,BBRP} = 4\pi R_P^2 \bar{\sigma} T_P^4 \tag{8}$$

where $L_{P,BBRP}$ is the luminosity, $\bar{\sigma} = 5.670370 \times 10^{-8}\ \mathrm{W/(m^2K^4)}$ is the Stefan-Boltzmann constant, T_P is the planet mean surface temperature and R_P its radius. Such radiation is assumed to be emitted radially from the planet.

Moreover, as defined by McInnes [1] and De Iuliis et al. [6], by considering planets as finite angular-sized discs with uniform brightness, the BBRP can be defined as:

$$P_{BBRP}(r) = \frac{L_{P,BBRP}}{3c\pi R_P^2}\left\{1 - \left[1 - \left(\frac{R_P}{r}\right)^2\right]^{\frac{3}{2}}\right\} \tag{9}$$

where $L_{P,BBRP}$ is the planetary luminosity and c is the speed of light.

The sail acceleration due to BBRP can be expressed as:

$$\boldsymbol{a}_{\boldsymbol{BBRP}} = a_B\left(\hat{\boldsymbol{u}}_{\boldsymbol{p}} \cdot \hat{\boldsymbol{n}}\right)^2 \hat{\boldsymbol{n}}$$

where $a_B = \frac{2P_{BBRP}\eta_{BBRP}}{\sigma}$.

Finally, by substituting the expressions of $\hat{\boldsymbol{u}}_{\boldsymbol{s}}$ and $\hat{\boldsymbol{n}}$ in Eq. (5) into Eq. (6) and by considering that $\alpha_N = \alpha_{sun} - \alpha$, the full expression for the sail acceleration due to BBRP is:

$$\begin{aligned}\boldsymbol{a}_{\boldsymbol{BBRP}} &= a_B \cos^2\alpha_N \begin{bmatrix}\cos\alpha_N \\ \sin\alpha_N\end{bmatrix} \\ &= a_B \begin{bmatrix}(\cos\alpha_{sun}\cos\alpha + \sin\alpha_{sun}\sin\alpha)^3 \\ (\cos\alpha_{sun}\cos\alpha + \sin\alpha_{sun}sin\alpha)^2(\sin\alpha_{sun}\cos\alpha - \cos\alpha_{sun}\sin\alpha)\end{bmatrix}\end{aligned} \tag{10}$$

3. Optimal Steering Law

The aim of this section is to determine the optimal steering law that maximises the increase of the semi-major axis by considering both SRP and BBRP. As a result, an optimal attitude of the sail, defined by the angle α, can be obtained for each position of the sail along its orbit.

The motion of the sail is studied in order to maximise the semi-major axis $a_f = a(t_f)$ at the final given time t_f. Therefore, following the Pontryagin's Minimum Principle [14], this corresponds to minimising the cost function $J = -a_f$.

The problem is strictly dependent on the illumination conditions that the sail has along its orbit and two main regions can be identified: the sunlit and the eclipse regimes.

3.1. Dynamical model

3.1.1. Sunlit regime

In order to find the optimal steering law that maximises the semi-major axis raise by using both the SRP and BBRP, the Hamiltonian of the problem H as well as the Lagrange-multipliers $\lambda_r, \lambda_u, \lambda_v$ and λ_θ are introduced. The Hamiltonian is defined as [14]:

$$H = \lambda_r u + \lambda_u \left(\frac{v^2}{r} - \frac{\mu_p}{r^2} + \right) + \lambda_v \left(- \frac{uv}{r} \right) + \lambda_\theta \frac{v}{r} + (\cos^2 \alpha \left((A + C) \cos\alpha + (B + D) \sin\alpha \right) + \sin^2 \alpha \, (E \cos\alpha + F \sin\alpha) \tag{11}$$

where:

$A = \lambda_u a_0 \cos\alpha_{sun} + \lambda_v a_0 \sin\alpha_{sun}$,

$B = \lambda_u a_0 \sin\alpha_{sun} - \lambda_v a_0 \cos\alpha_{sun}$,

$C = \lambda_u a_B \cos^3 \alpha_{sun} + \lambda_v a_B \cos^2 \alpha_{sun} \sin\alpha_{sun}$,

$D = 3\lambda_u a_B \cos^2 \alpha_{sun} \sin\alpha_{sun} - \lambda_v a_B \cos^3 \alpha_{sun} + 2\lambda_v a_B \sin^2 \alpha_{sun} \cos\alpha_{sun}$,

$E = 3\lambda_u a_B \sin^2 \alpha_{sun} \cos\alpha + \lambda_v a_B \sin^3 \alpha_{sun} - 2\lambda_v a_B \cos^2 \alpha_{sun} \sin\alpha_{sun}$,

$F = \lambda_u a_B \sin^3 \alpha - \lambda_v a_B \sin^2 \alpha_{sun} \cos\alpha_{sun}$.

By applying the Euler-Lagrange theorem [14], the optimal control can be found by solving the following equation involving the first-order derivative of the Hamiltonian H with respect to the control angle α:

$$\frac{\partial H}{\partial \alpha} = 0 \tag{12}$$

By substituting Eq. (11) into Eq. (12), the following equation is obtained:

$$-E \tan\alpha + (-2(B + D) + 3F) \tan^2 \alpha + (-3(A + C) + 2E) \tan\alpha + (B + D) = 0 \tag{13}$$

Solving this equation gives three different values of the control angle α, and the Minimum Principle can be numerically applied in order to determine which angle minimises the Hamiltonian defined by Eq. (11).

Furthermore, as A, B, C, D, E and F depend on the Lagrange multipliers, the costate equations must be determined. Starting from the boundary conditions at the final time, the costate equations are solved backwards in time to obtain the initial values which maximise the final semi-major axis. These equations are defined as follows:

$$\dot{\boldsymbol{\lambda}} = -\frac{\partial H}{\partial \boldsymbol{x}} \tag{14}$$

Using Eq. (11), one can obtain:

$$\begin{aligned}\dot{\lambda_r} = \lambda_u \left(\frac{v^2}{r^2} - \frac{2\mu_p}{r^3} - \frac{2L_{P,BBRP}\,\eta_{BBRP}}{\sigma c \pi r^3} \cos^3(\alpha+\theta) \left(1 - \frac{{R_P}^2}{r^2}\right)^{\frac{1}{2}} \right) \\ - \lambda_v \left(\frac{uv}{r^2} - \frac{2L_{P,BBRP}\,\eta_{BBRP}}{\sigma c \pi r^3} (\cos^2(\alpha+\theta) \sin(\alpha+\theta) \left(1 - \frac{{R_P}^2}{r^2}\right)^{\frac{1}{2}} \right) + \lambda_\theta \frac{v}{r^2}\end{aligned} \tag{15}$$

$$\dot{\lambda_u} = \frac{\lambda_v v}{r} - \lambda_r \tag{16}$$

$$\dot{\lambda_v} = -\frac{\lambda_\theta - \lambda_v u + 2\lambda_u v}{r} \tag{17}$$

$$\begin{aligned}\dot{\lambda_\theta} = -\lambda_v \cos(\alpha+\theta) \left(\left(\frac{P_{sun}}{2}(\cos(2\alpha)+1\right) \right. \\ \left. - \frac{2L_{P,BBRP}\,\eta_{BBRP}}{3{R_P}^3 \sigma c \pi} \left(\left(1 - \frac{{R_P}^2}{r^2}\right)^{\frac{3}{2}} - 1 \right) (\cos^2(\alpha+\theta) + 2\sin^2(\alpha+\theta)) \right) \\ - \lambda_u \sin(\alpha+\theta) \left(\left(\frac{P_{sun}}{2}(\cos(2\alpha+\theta)+1)\right) \right. \\ \left. - \frac{2L_{P,BBRP}\,\eta_{BBRP}}{{R_P}^2 \sigma c \pi} \left(\left(1 - \frac{{R_P}^2}{r^2}\right)^{\frac{3}{2}} - 1 \right) \cos^2(\alpha+\theta) \right)\end{aligned} \tag{18}$$

3.1.2. Eclipse regime

When the sail is in eclipse, only the BBRP acts on the sailcraft. Hence, forces acting on the sail are different from the sunlit case and a new steering law must be calculated. The same method as the one developed in Subsection 3.1.1

has been followed. The Hamiltonian defined in Eq. (11) is modified by setting the coefficients A and B (which represent the contribution of SRP) equal to zero:

$$H = \lambda_r u + \lambda_u \left(\frac{v^2}{r} - \frac{\mu_p}{r^2} +\right) + \lambda_v \left(-\frac{uv}{r}\right) + \lambda_\theta \frac{v}{r} + (\cos^2\alpha\,(C\cos\alpha + D\sin\alpha) + \sin^2\alpha\,(E\cos\alpha + F\sin\alpha) \tag{19}$$

Similarly, Eq. (13) is modified, and the optimal control angle can be found by applying the Minimum Principle to the following equation:

$$-E\tan\alpha + (-2D + 3F)\tan^2\alpha + (-3C + 2E)\tan\alpha + D = 0 \tag{20}$$

As the contribution of the SRP on the sail does not depend on r, u and v, the costate equations linked to these variables, Eqs. (15), (16) and (17) respectively, remain unchanged for the eclipse regime. The costate equation linked to θ is determined from Eq. (14) and is written as:

$$\dot{\lambda_\theta} = \frac{2L_{P,BBRP}\,\eta_{BBRP}}{3{R_P}^2\sigma c\pi}\left(\left(1 - \frac{{R_P}^2}{r^2}\right)^{\frac{3}{2}} - 1\right)(3\lambda_v\cos^3(\alpha+\theta) - 2\lambda_v\cos(\alpha+\theta) + 3\lambda_u\cos^2(\alpha+\theta)\sin(\alpha+\theta)) \tag{21}$$

3.2. Boundary Conditions

Boundary conditions are needed to complete the two-point boundary value problem. Five initial conditions are already known: r_0, u_0, v_0, θ_0 and t_0. Moreover, the problem is formulated in such a way that the final time t_f is known. The four remaining boundary conditions associated with r_f, u_f, v_f and θ_f are found using the Euler-Lagrange theorem, from the transversality condition [14]:

$$-\lambda_{r_f} - \frac{\frac{2}{r_f^2}}{\left(\frac{\sqrt{u_f^2 + v_f^2}}{\mu_P} - \frac{2}{r_f}\right)^2} = 0 \tag{22}$$

$$-\lambda_{u_f} - \frac{\frac{u_f}{\mu_p\sqrt{u_f^2 + v_f^2}}}{\left(\frac{\sqrt{u_f^2 + v_f^2}}{\mu_P} - \frac{2}{r_f}\right)^2} = 0 \tag{23}$$

$$-\lambda_{v_f} - \frac{\frac{v_f}{\mu_p\sqrt{u_f^2+v_f^2}}}{\left(\frac{\sqrt{u_f^2+v_f^2}}{\mu_P}-\frac{2}{r_f}\right)^2} = 0 \tag{24}$$

$$\lambda_{\theta_f} = 0 \tag{25}$$

Finally, the state and costate functions of both the sunlit regime and the eclipse regime provide a complete two-point boundary value problem (BVP) which can be solved numerically. In this study, the BVP is solved numerically using the *bvp4c* function in MATLAB®.

4. Numerical Results

Numerical simulations have been carried out in order to assess the performance of the new steering law, that will be called *optimal steering law SRP+BBRP* in this section. In order to estimate the efficiency of this law, a comparison with two other steering laws has been made:

- *optimal steering law SRP only:* an optimal steering law that only considers the effect of the SRP to increase the final semi-major axis, based on Pontryagin's principle when the sail is in sunlit conditionsThe same law is then used in the eclipse region even though SRP is not considered in the propagation of the trajectory of the sail.
- *on-off switching law*: as defined by McInnes [1], where the sail is perpendicular to the solar rays for half of the orbit and parallel to it for the other half of the orbit.

It is important to note that all the simulations include both SRP and BBRP in the propagation of the trajectory of the sail, regardless of the steering law applied to the system. Table 1 summarises the radiation pressure sources considered in the three steering laws.

Table 1 Summary of the steering laws and radiation pressure sources considered

	Optimal law		Non-optimal law
	Optimal steering law SRP+BBRP	*Optimal steering law SRP only*	*On-off switching law*
Propagation of the sail in sun light	SRP + BBRP	SRP + BBRP	SRP + BBRP
Propagation of the sail in eclipse	BBRP	BBRP	BBRP
Optimisation of the steering law	SRP + BBRP	SRP	No optimisation

The initial conditions applied to Eqs. (1), (2), (3) and (4) are: $\boldsymbol{x}_0(t_0) = \begin{bmatrix} R_P + h_0 & 0 & \sqrt{\frac{\mu_p}{r_0}} & 0 \end{bmatrix}^T$, where R_P is the planetary radius and h_0 is the initial altitude of the sail.

The performance of the four different steering laws is evaluated by the percentage increase in semi-major axis after one revolution, following the formula:

$$\Delta a = 100\left(\frac{a_f}{R_P + h_0} - 1\right) \tag{26}$$

where a_f is final semi-major axis of the orbit.

Moreover, the performance of the *optimal steering law SRP+BBRP* is also evaluated in terms of percentage gain in semi-major axis increase compared to the *optimal steering law SRP only* as:

$$\Delta g = 100\left(\frac{\Delta a_{SRP+BBRP}}{\Delta a_{SRP\ only}} - 1\right) \tag{27}$$

Analyses have been conducted considering a double-sided reflective coating such that both front side and back side of the sail have the same optical properties. An optical efficiencies are set $\eta_{SRP} = \eta_{BBRP} = 0.85$ for both the solar and black-body radiation. These values approximate the behavior of Aluminum, whose reflectivity varies by only 12% in the range of wavelengths between 300 nm (sunlight) and 2500 nm (infraread)[16]. A parametric analysis showing the performance of the sail with different optical properties will be then shown in Section 4.3.

Analyses have been performed for Earth and Venus. The main parameters for these two planets are summarised in Table 2.

Table 2 Parameters for the Earth and Venus scenarios

	P_{sun}, N/m^2	R_P, m	T_P, K	$L_{P,BBRP}$, W	μ_p, m^3/s^2
Earth	4.56×10^{-6}	6371×10^3	279.00	1.756×10^{17}	398604.3×10^9
Venus	8.72×10^{-6}	6070×10^3	735.15	7.668×10^{18}	324859×10^9

Different initial altitudes h_0 have been considered for Earth and Venus. Moreover, different values for the solar sail loading σ have been analysed, $\sigma = 77.5\ \text{g/m}^2, 31\ \text{g/m}^2, 15.5\ \text{g/m}^2, 7.8\ \text{g/m}^2$ and $5.2\ \text{g/m}^2$, which correspond to the following characteristic accelerations respectively: $a_0 = 0.1\ \text{mm/s}^2, 0.25\ \text{mm/s}^2, 0.5\ \text{mm/s}^2, 1\ \text{mm/s}^2$ and $1.5\ \text{mm/s}^2$. For reference, the recent NASA mission study Sunjammer[†] used $a_0 = 0.06\ mm/s^2$, therefore it

[†] https://www.nasa.gov/mission_pages/tdm/solarsail/index.html

is reasonable to consider a modest development in technology leading to $a_0 = 0.1\ mm/s^2$, and up to $2\ mm/s^2$ for far-term solar sails

4.1. Performance evaluation of optimal steering law

4.1.1. Earth

The evaluation of the performance of the *optimal steering law SRP+BBRP* around the Earth is presented in this section. Fig. 2 represents the evolution of the semi-major axis for a sail characterised by $\sigma = 7.8\ g/m^2$, orbiting around the Earth for a starting altitude $h_0 = 800\ km$, for the three steering laws taken into account in this study. The area in between the two vertical lines represents the period in which the sail is in eclipse.

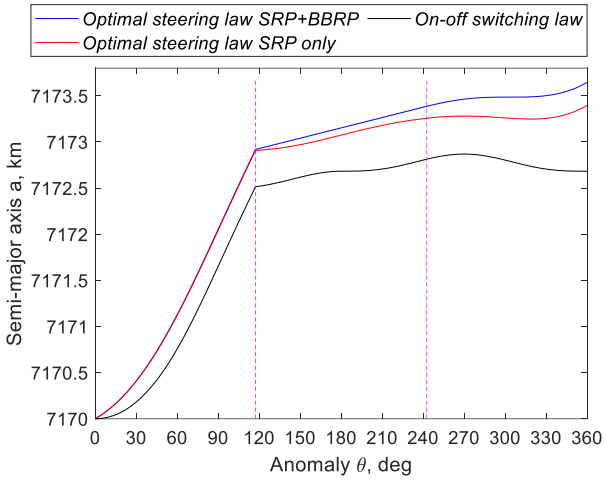

Fig. 2 Evolution of the semi-major axis over one revolution for a sail orbiting around the Earth, starting at $h_0 = 800$ km, for different control laws

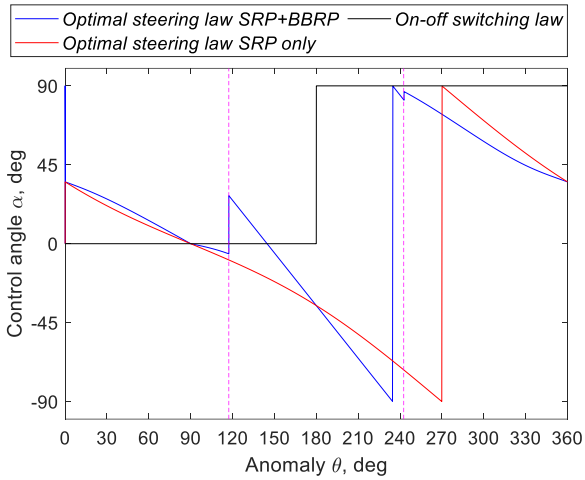

Fig. 3 Evolution of the control angle α over one revolution for a sail orbiting around the Earth, starting at $h_0 = 800$ km, for different control laws

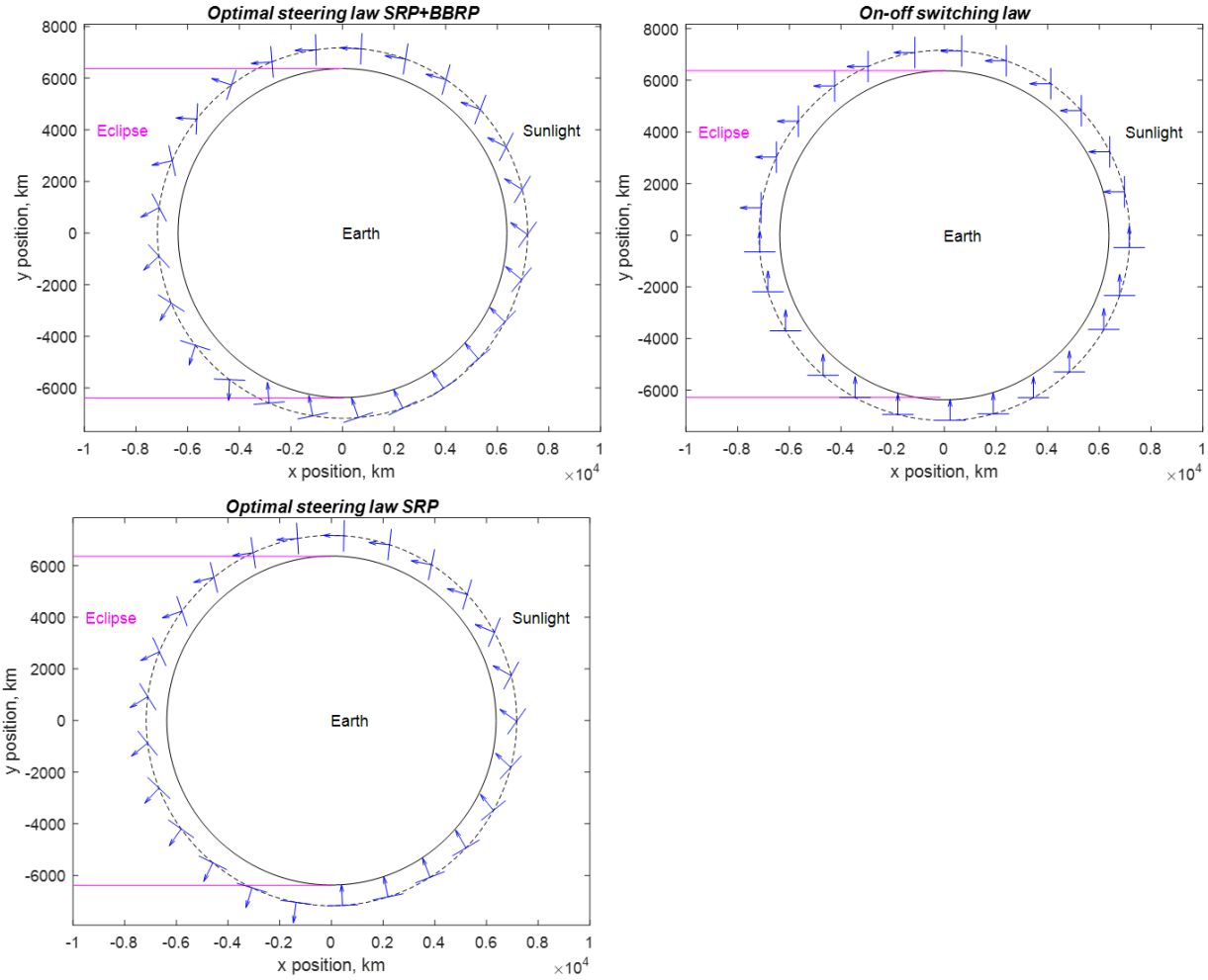

Fig. 4 Trajectory and orientation of the sail around the Earth for different steering laws

Fig. 2 shows a sensible improvement of the performance of the sail when BBRP is considered. Indeed, the comparison between the *optimal steering law SRP only* (red line) and the *optimal steering law SRP+BBRP* (blue line) shows that a higher final semi-major axis is achieved with the *optimal steering law SRP+BBRP*. As expected, the main difference is observed during the eclipse: the *optimal steering law SRP+BBRP* succeeds in producing a higher increase of altitude by optimising the energy received from the BBRP, while the *optimal steering law SRP only*, shows a lower efficiency in this phase. This leads to a gain in semi-major axis increase of 7.17% compared to the *optimal steering law SRP only*, as shown in Table 3.

The evolution of the control angle α during one orbit is shown in Fig. 3 and Fig. 4. It is to note that the switch in sign for α from -90° to +90° in Fig. 3 is only due to the definition of its bound in Sec. 2.1; it does not involve any attitude change as shown in Fig. 4 (as the optical properties of the sail are the same on both sides, a flip of 180° is irrelevant). As for the behaviour of the semi-major axis mentioned above, the main difference in the evolution of the control angle between the *optimal steering law SRP only* and the *optimal steering law SRP+BBRP* appears during the eclipse. While α varies in a smooth and similar way for the *optimal steering law SRP only* and the *optimal steering law SRP+BBRP* before the sail enters into eclipse, the *optimal steering law SRP+BBRP* reorients the sail during the eclipse, in order to maximise the acceleration due to BBRP. When the sail leaves the eclipse and moves towards the Sun, the *optimal steering law SRP+BBRP* orients the sail in a such way to gain momentum from the BBRP while minimising the one obtained by SRP.

The same profile of control angle is also obtained with other starting altitudes. Table 2 summarises the obtained results for $h_0 = 800, 1000, 5000$ and 30000 km.

The *optimal steering law SRP+BBRP* and the *optimal steering law SRP only*, enable larger increases in semi-major axis compared to the sub-optimal law shown in the first column of Table 3. The percentage gain in semi-major axis of the *optimal steering law SRP+BBRP* compared to the *optimal steering law SRP only* (Δg) is shown in the last column of Table 3. It is worth noting that the effects of the BBRP are greater when the sail is closer to the Earth, while starting from the altitude $h_0 = 5000$ km such a gain becomes negligible.

Table 3 Performance of steering laws for the Earth case

Initial altitude, km	Increase in semi-major axis after one orbit (Δa)			Gain in semi-major axis increase of SRP+BBRP compared to SRP (Δg)
	On-off switching law	*Optimal steering law SRP only*	*Optimal steering law SRP+BBRP*	
800	$3.74 \times 10^{-2}\%$	$4.74 \times 10^{-2}\%$	$5.08 \times 10^{-2}\%$	7.17%
1000	$4.07 \times 10^{-2}\%$	$5.13 \times 10^{-2}\%$	$5.47 \times 10^{-2}\%$	6.63%
5000	$1.18 \times 10^{-1}\%$	$1.48 \times 10^{-1}\%$	$1.50 \times 10^{-1}\%$	1.35%
30000	1.33%	1.78%	1.78%	0%

4.1.2. Venus

A similar analysis has been conducted for a sail orbiting around Venus where the BBRP might have comparable magnitudes as the SRP in a certain range of altitudes. Indeed, Fig. 5 shows the magnitudes of the ARP, BBRP and SRP with respect to different altitudes for the Earth and Venus cases. It is worth noting that ARP remains limited in both cases, but BBRP is the dominant radiation for altitudes below $15000\ km$ in the Venus case.

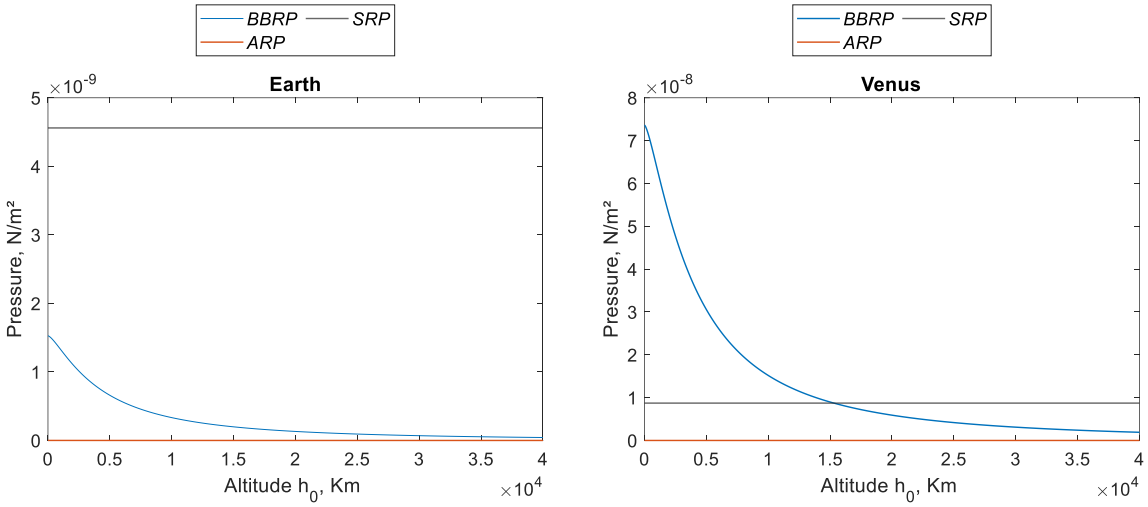

a) b)

Fig. 5 Magnitude of radiation pressures in a) Earth and b) Venus case depending on the altitude

Fig. 6 shows the evolution of the semi-major axis for a sail orbiting around Venus, starting at $h_0 = 800\ km$, for the different steering laws. It clearly appears that the *optimal steering law SRP+BBRP* guarantees better performances in terms of the increase of the semi-major axis over one revolution compared to the other two steering laws. Fig. 7 shows the evolution of the control angle α for a sail orbiting around Venus, starting from $h_0 = 800$ km, for the three

different steering laws. In contrast with the Earth case, during the sunlit regime, the control angle α of the *optimal steering law SRP+BBRP* varies in a similar way to the one used during the eclipse regime. Indeed, apart from a reorientation of the sail by a few degrees, the attitude of the sail does not change between the sunlit region and the eclipse region.

Table 4 summarises the obtained results for both different altitudes and different steering laws. Despite the intensity of BBRP decreases when the sail is farther from the planet, the gain in semi-major axis increase due to BBRP is substantial for a large range of starting altitudes and can be up to 853% for $h_0 = 800$ km.

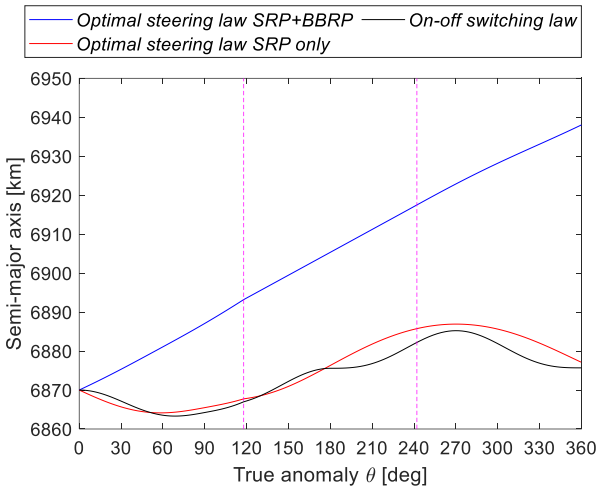

Fig. 6 Evolution of the semi-major axis over one revolution for a sail orbiting around Venus, starting at $h_0 = 800$ km, for different control laws

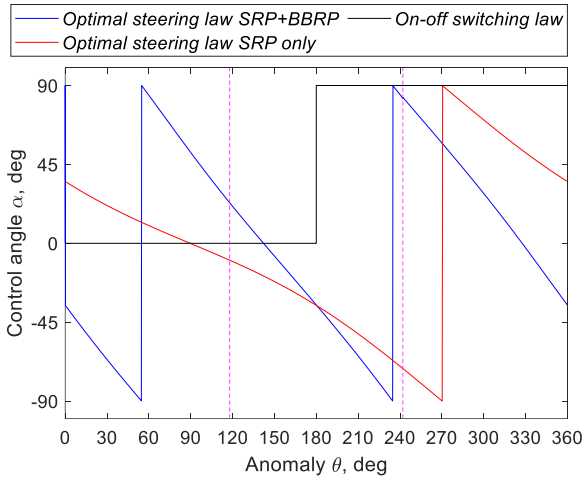

Fig. 7 Evolution of the control angle α over one revolution for a sail orbiting around Venus, starting at $h_0 = 800$ km, for different control laws.

Table 4 Steering laws performances for the Venus case

Initial altitude, km	Increase in semi-major axis (Δa)			Gain in semi-major axis increase of SRP+BBRP compared to SRP (Δg)
	On-off switching law	*Optimal steering law SRP only*	*Optimal steering law SRP+BBRP*	
800	$8.29 \times 10^{-2}\%$	$1.04 \times 10^{-1}\%$	$9.91 \times 10^{-1}\%$	853%
1000	$9.04 \times 10^{-2}\%$	$1.12 \times 10^{-1}\%$	1.01%	802%
5000	$2.67 \times 10^{-1}\%$	$3.31 \times 10^{-1}\%$	1.19%	261%
30000	3.16%	4.20%	4.38%	4.29%

4.2. Effect of the solar sail loading

The effect of varying the sail loading σ is now investigated. Fig. 8 and Fig. 9 report the percentage gain in semi-major axis increase Δg per orbit of the *optimal steering law SRP+BBRP* compared to the *optimal steering law SRP only*, for different solar sail loadings and different starting altitudes h_0, in both Earth and Venus orbits.

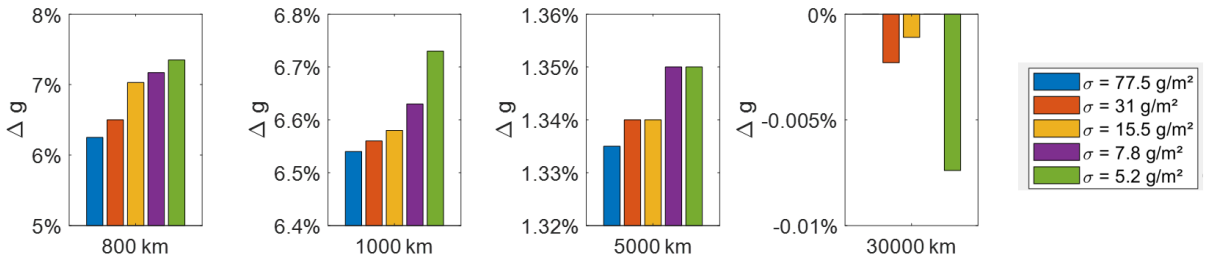

Fig. 8 Percentage gain in semi-major axis increase for different solar sail loading σ, at different starting altitude h_0, in Earth orbit.

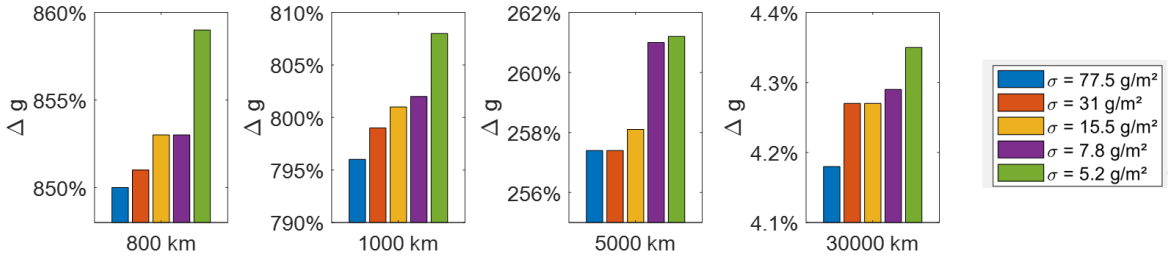

Fig. 9 Percentage gain in semi-major axis increase for different solar sail loading σ, at different starting altitude h_0, in Venus orbit.

As expected, for both Earth and Venus cases and for all starting altitudes, the smaller the solar sail loading, the larger the gain in semi-major axis increase. It is worth noting that, in Earth orbit, for $h_0 = 30000\ km$, the gain in semi-major increase is slightly negative. However, the difference in percentage between the two steering laws is very small and falls within the uncertainty of the model. Therefore, it can be concluded that the two steering laws (both the *optimal steering law SRP+BBRP* and the *optimal steering law SRP only*) give the same results in such regions where the main contribution is given by SRP.

4.3. Effect of the reflectivity coefficient

The reflectivity of each material varies depending on the wavelength of the emitted source. The aim of this subsection is to study the effect of the coating on the performance of the sail. Three different materials are studied, i.e., aluminium, vaporized deposited gold and white paint S13G-LO. Table 5 summarises the optical properties of each material [5]. The second and the third column of the table show the values of the absorbivity in the visible region of the spectrum ($380nm$ to $700nm$) , A_{SRP}, and emissivity in the infrared part of the spectrum (from $10\mu m$ to $1mm$ wavelength), E_{BBRP}, that are used to calculate the reflectivity of the sail for the SRP and BBRP, respectively. In accordance with the Wien's law [5], the major energy contributions from the sun and the planet are in the visible and infrared parts of the spectrum, respectively. The SRP reflectivity, η_{SRP}, accounts for the part of the visible spectrum that is not absorbed by the material. Consequently, it can be calculated as:

$$\eta_{SRP} = 1 - A_{SRP} \tag{28}$$

The BBRP reflectivity, η_{BBRP}, can be defined as the part of the infrared radiation that is not absorbed by the material. In accordance with Kirchhoff's law of thermal radiation [17], the absorbivity and emissivity of materials have same values at the same part of the spectrum, so that $A_{BBRP} = E_{BBRP}$ at the infrared wavelength. Therefore, the reflectivity of the BBRP can be calculated as follows:

$$\eta_{BBRP} = 1 - A_{BBRP} = 1 - E_{BBRP} \tag{29}$$

The values obtained from Eqs. (28) and (29) are reported in the last two columns of Table 5 and will be used to perform the parametric analyses in this section.

Table 5 Optical properties of materials [5]

Material	SRP absorptivity* (A_{SRP})	BBRP emissivity** (E_{BBRP})	SRP reflectivity (η_{SRP})	BBRP reflectivity (η_{BBRP})
Aluminum	0.15	0.15	0.85	0.85
Vaporized Deposited Gold	0.3	0.03	0.7	0.97
White paint S13G-LO	0.25	0.85	0.75	0.15

* visible spectrum ($380nm$ to $700nm$)
** infrared spectrum(from $10\mu m$ to $1mm$ wavelength)

Fig. 10, Fig. 11 and Fig. 12 show the evolution of the semi-major axis over one revolution of a solar sail characterised by $\sigma = 7.8\ \mathrm{g/m^2}$, on Earth and Venus orbits, for $h_0 = 800$ km, $h_0 = 5000$ km and $h_0 = 30000$ km respectively and for the three different materials.

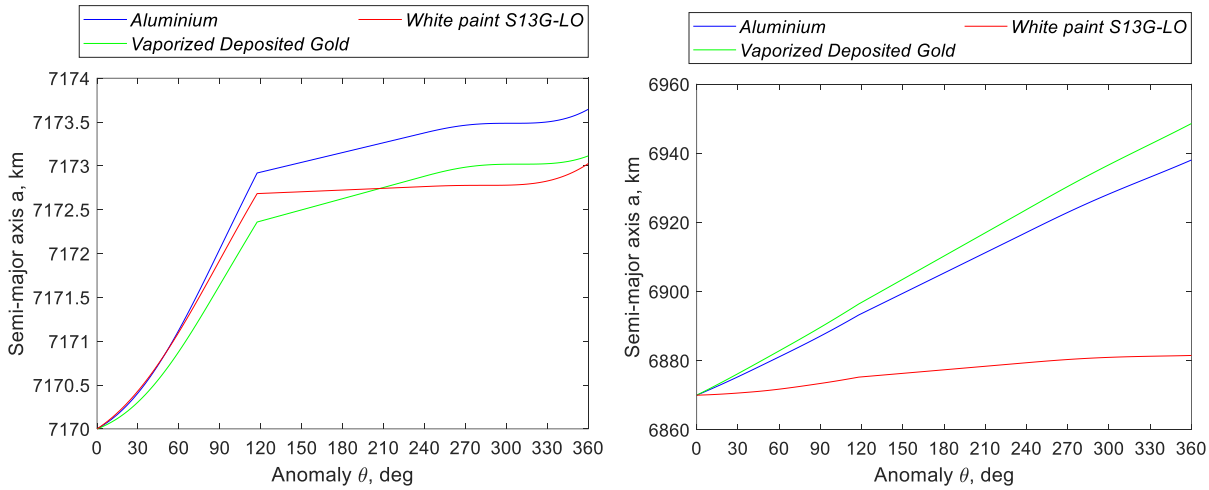

(a) (b)

Fig. 10 Evolution of the semi-major axis for a sail orbiting around Earth (a) and Venus (b) over one revolution, depending on the coating of the sail, at $h_0 = 800$ km.

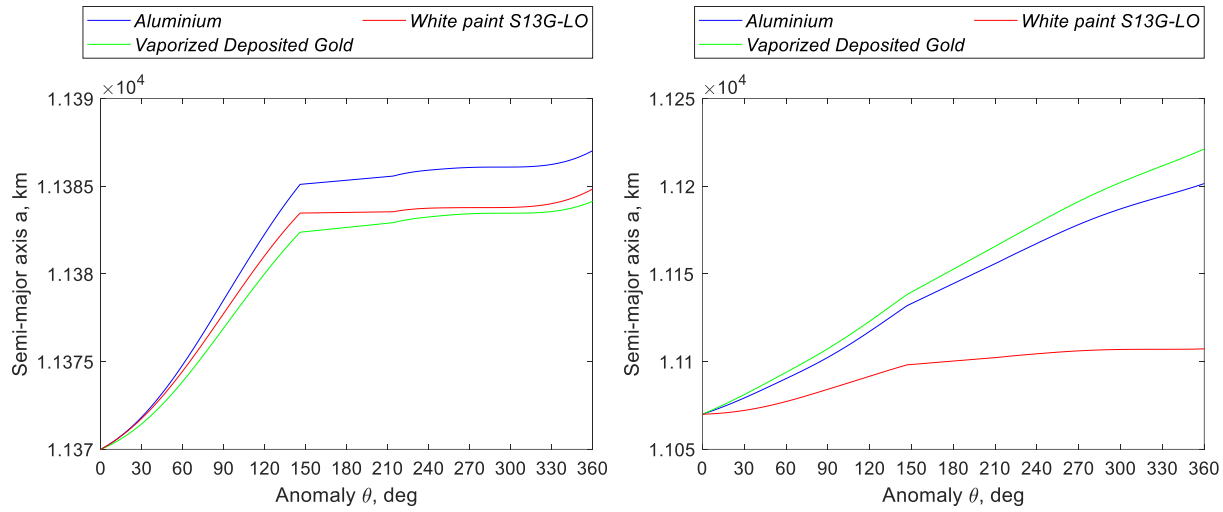

(a) (b)

Fig. 11 Evolution of the semi-major axis for a sail orbiting around Earth (a) and Venus (b) over one revolution, depending on the coating of the sail, at $h_0 = 5000$ km.

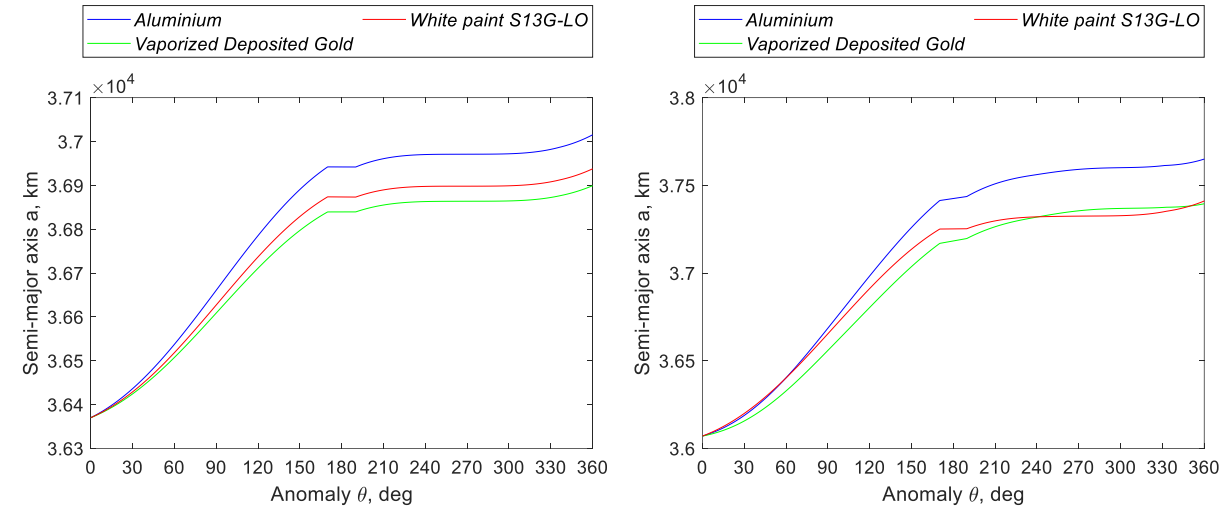

(a) (b)

Fig. 12 Evolution of the semi-major axis for a sail orbiting around Earth (a) and Venus (b) over one revolution, depending on the coating of the sail, at $h_0 = 30000$ km.

In Earth orbit, above $h_0 = 800\ km$, even if the sail allows a greater reflectivity for BBRP than SRP by using Vaporized Deposited Gold, the final semi-major axis is smaller than that obtained with White paint S13G-LO which gives a greater reflectivity for SRP than for BBRP. This is not the case when the sail is orbiting around Venus. Indeed, for $h_0 = 800$ km and $h_0 = 5000$ km, increasing the reflectance of BBRP compared to SRP allows the sail to reach a larger final semi-major axis, as shown in Fig. 10 and Fig. 11. However, for higher altitudes, such as $h_0 = 30000$ km for the Venus case shown in Fig. 12, the SRP becomes the dominant contribution and therefore the performance of

the sail will be mostly affected by the values of reflectance of SRP. This confirms that each planet has its own limit zone where the contribution of BBRP is dominant compared to solar radiation as shown in Fig. 5. For planets where the BBRP is significant, considering a solar sail's reflectivity greater for BBRP than for SRP still gives better results in low orbits.

4.4. Long Term Orbit Raising

Analyses have been conducted with a sail orbiting around Earth and Venus for 24 hours, covered with Aluminum such that $\eta_{SRP} = \eta_{BBRP} = 0.85$ and with a solar sail loading $\sigma = 7.8\ \mathrm{g/m^2}$. Fig. 13 shows the evolution of the semi-major axis for a sail orbiting around Earth and Venus for one day, starting at $h_0 = 800$ km.

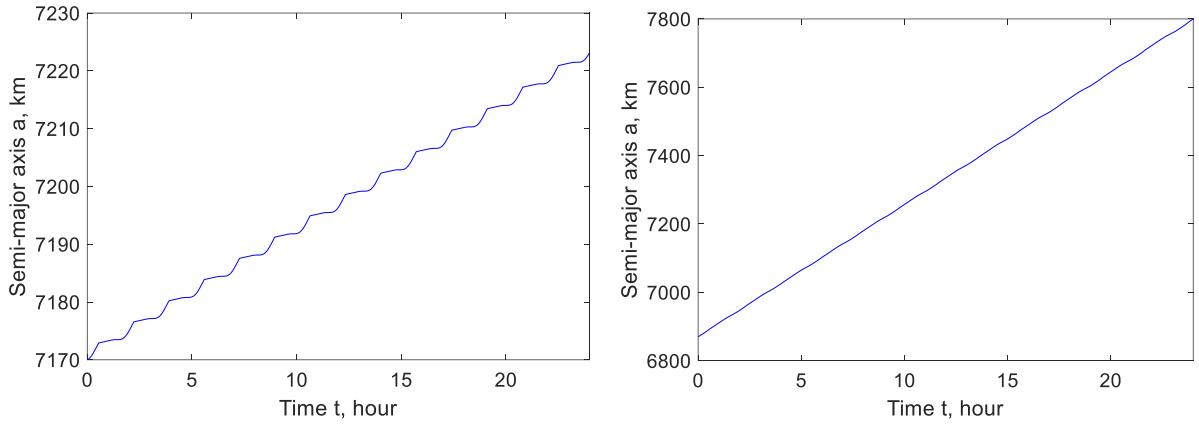

(a) (b)

Fig. 13 Evolution of the semi-major axis of a sail orbiting around Earth (a) and Venus (b), for 24 hours, at starting altitude $h_0 = 800\ km$

The evolution of the semi-major axis is quasi-linear for a sail orbiting around Venus and leads to an increase of the semi-major axis of 918.6 km. Fig. 14 summarises the results obtained in semi-major axis increase for different starting altitudes for both Earth and Venus. In Earth orbit, the higher the initial altitude, the larger the semi-major axis increase. This is not the case for Venus where the increase in semi-major axis at $h_0 = 800$ km is higher than for $h_0 = 5000$ km but is lower than for $h_0 = 30000$ km. The altitudes $h_0 = 500$ km and $h_0 = 5000$ km belong to the zone where BBRP is the dominant force. Moreover, this force is inversely proportional to the distance from the planet. Hence, the increase in semi-major axis is decreasing when the attitude is increasing. When SRP becomes the dominant contribution, the increase in semi-major axis is increasing with initial altitudes. It is worth to note that due to the

simulation time set to 24 hours, the increase in semi-major axis is not continuously increasing with respect to the starting altitude. Indeed, depending on the orbit period, the trajectory ends in a favourable or in a less favourable part of the revolution.

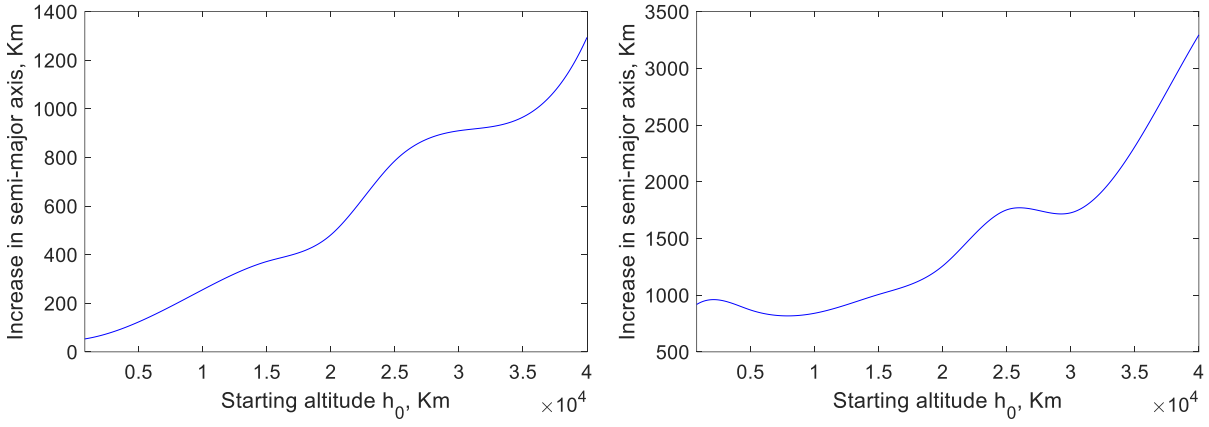

a) b)

Fig. 14 Semi-major axis increase over one day for Earth (a) and Venus (b) depending on the starting altitude

5. Conclusion

This work proposed an optimal steering law for orbit raising of sails exploiting both Solar Radiation Pressure (SRP) and Black-Body Radiation Pressure (BBRP). As the force induced by the sail varies with its position relative to the planet, the steering law is optimised for the sunlit and the eclipse regimes, using an indirect approach. The algorithm switches between the two different control laws during the integration of the equations of motion. Numerical analyses have been performed around Earth and Venus in two-dimensional scenarios. Results are compared to steering laws which consider SRP only. In the Earth case, results show that there is no substantial difference with an optimal law considering SRP only to increase semi-major axis. However, when the sail is orbiting around Venus, BBRP becomes the dominant force and allows for a sensible orbit raising. For a sail with loading of 7.8 g/m^2, starting at an altitude of 800 km, in Earth orbit, the percentual increase in semi-major axis after one revolution is 1.35 times higher using an optimized steering law considering both SRP and BBRP compared to an optimized steering considering only SRP and it is up to 9.52 times higher in Venus orbit. The difference between Earth and Venus is mainly due to the

difference in surface temperature between the two planets, which leads to a BBRP up to 48 times higher in Venus orbit than in the Earth's. Moreover, this study highlights that the choice of both solar sail loading and sail coating material can lead to an improvement of the performance in orbit raising for both Earth and Venus.

References

[1] McInnes C., *Solar Sailing: Technology, Dynamics and Mission Applications*, Praxis Publishing Ltd, Chichester, UK, 1999

[2] Gong S., Macdonald M., "Review on solar sail technology", *Astrodynamics*, 2019, Vol. 3, pp. 93-125, DOI: 10.1007/s42064-019-0038-x

[3] Macdonald M., McInnes C., "Solar sail science mission applications and advancement", *Advances in Space Research*, 2011, Vol 48, No. 11, pp. 1702-1716, DOI: 10.1016/j.asr.2011.03.018

[4] Macdonald M., McInnes C., Alexander D., Sandman A., "GeoSail: exploring the magnetosphere using a low-cost solar sail", *5th IAA International conference on Low-Cost Planertary Missions*, ESTEC, Noordwijk, The Netherlands, 2003

[5] Larson, W. J. and Wertz, J. R., *Space Mission Analysis and Design*, 3rd ed, Microcosm Press, California, 2006

[6] De Iuliis A., Ciampa F., Felicetti L., Ceriotti M., "Sailing with solar and planetary radiation pressure", *Advances in Space Research*, Vol. 67, No. 9, December 2019, DOI: 10.1016/j.asr.2019.11.036

[7] Fieseler P., "A Method for Solar Sailing in a Low Earth Orbit" *Acta Astronautica*, Vol. 43, No. 9-10, pp. 531-541, 1998

[8] Macdonald M., McInnes C., "Analytical Control Laws for Planet-Centered Solar Sailing", *Journal of Guidance, Control and Dynamics*, Vol. 28, No. 5, September-October 2005, DOI: 10.2514/1.11400

[9] Macdonald M., McInnes C., "Realistic Earth Escape Strategies for Solar Sailing", *Journal of Guidance, Control and Dynamics*, Vol. 28, No.2, March-April 2005, DOI: 10.2514/1.5165

[10] Mengali G., Quarta A., "Near-Optimal Solar-Sail Orbit-Raising from Low Earth Orbit", *Journal of Spacecraft and Rockets*, Vol.42, No. 5, September-October 2005, DOI: 10.2514/1.14184

[11] Mengali G., Quarta A., "Earth Escape by Ideal Sail and Solar-Photon Thrustor Spacecraft", *Journal of Guidance, Control and Dynamics*, Vol. 27, No. 6, pp. 1105-1108, DOI: 10.2514/1.10637

[12] Stolbunov V., Ceriotti M., Colombo C., McInnes C., "Optimal law for Inclination Change in an Atmosphere Through Solar Sailing", *Journal of Guidance, Control and Dynamics*, Vol. 36, No. 5, September-October 2013, DOI: 10.2514/1.59931

[13] Felicetti L., Ceriotti M., Harkness P., "Attitude Stability and Altitude Control of a Variable-Geometry Earth-Orbiting Solar Sail", *Journal of Guidance, Control and Dynamics*, Vol. 39, No. 9, September 2016, DOI: 10.2514/1.G001833

[14] Longuski J. M., Guzmán J. J., Prussing J. E., *Optimal Control with Aerospace Applications*, Springer, Heidelberg, 2014, DOI: 10.1007/978-1-4614-8945-0

[15] Bryson A. E., Ho Y.C., *Applied Optimal Control*, Taylor & Francis Group, New York, 1975

[16] Bass M., DeCusatis C., Enoch J., Lakshminarayanan V., Li G., Macdonald C., Mahajan V., Van Stryland E., *Handbook of optics, Volume II: Design, Fabrication and Testing, Sources and Detectors, Radiometry and Photometry*, McGraw-Hill Inc, New York, 2009

[17] M. Riedl, *Optical Design Fundamentals for Infrared Systems, Second Edition*, SPIE Press, Bellingham WA, 2001